Spectral analysis of RE^{3+} (RE = Er, Nd, Pr and Ho):GeO_2–B_2O_3–ZnO–LiF glasses

2008 J. Phys.: Condens. Matter 20 375104

(http://iopscience.iop.org/0953-8984/20/37/375104)

J. Phys.: Condens. Matter **20** (2008) 375104 (12pp) doi:10.1088/0953-8984/20/37/375104

Spectral analysis of RE^{3+} (RE = Er, Nd, Pr and Ho):GeO_2–B_2O_3–ZnO–LiF glasses

G Lakshminarayana[1,5], Jianrong Qiu[1], M G Brik[2], G A Kumar[3] and I V Kityk[4]

[1] State Key Laboratory of Silicon Materials, Zhejiang University, Hangzhou 310027, People's Republic of China
[2] Institute of Physics, University of Tartu, Riia 142, Tartu 51014, Estonia
[3] Department of Material Science and Engineering, The State University of New Jersey, NJ 08854-8065, USA
[4] Department of Chemistry, Silesian University of Technology, ulica Marcina Strzody 9, PL-44100 Gliwice, Poland

E-mail: glnphysics@rediffmail.com

Received 7 June 2008, in final form 1 August 2008
Published 26 August 2008
Online at stacks.iop.org/JPhysCM/20/375104

Abstract

This paper reports on the absorption, visible and near-infrared luminescence properties of Er^{3+}, Nd^{3+}, Pr^{3+} and Ho^{3+}-doped alkali fluoride zinc boro germanate glasses. The x-ray diffraction (XRD) and differential thermal analysis (DTA) profiles of the host glass have been carried out, to confirm its structure and thermal stability. From the measured absorption spectra, Judd–Ofelt (JO) intensity parameters (Ω_2, Ω_4 and Ω_6) have been calculated for all the studied ions. For Pr^{3+} and Ho^{3+}-doped glasses, upconversion emission spectra have also been measured. Decay curves were measured for the visible emissions of Er^{3+}, Pr^{3+} and Ho^{3+} ions at 547 nm (Er^{3+}: green), 604 nm and 641 nm (Pr^{3+}: orange and red) and 658 nm (Ho^{3+}: red), respectively. The near-infrared emission spectra of Er^{3+}/Yb^{3+} and Nd^{3+}-doped glasses have shown full width at half maximum (FWHM) around 95 nm (for the $^4I_{13/2} \rightarrow {}^4I_{15/2}$ transition) and 63 nm (for the $^4F_{3/2} \rightarrow {}^4I_{11/2}$ transition), respectively. The measured maximum decay times of $^4I_{13/2} \rightarrow {}^4I_{15/2}$ transition (at wavelength 1.51 μm) are about 5.72 ms and 6.14 ms for $1.0Er^{3+}$ and $1.0Er^{3+}/2Yb^{3+}$ (mol%)-codoped glasses, respectively. The maximum stimulated emission cross sections for $^4I_{13/2} \rightarrow {}^4I_{15/2}$ transition of Er^{3+} and Er^{3+}/Yb^{3+} are 5.447×10^{-21} cm^2 and 4.540×10^{-21} cm^2. These glasses with better thermal stability, bright visible emissions and broad near-infrared emissions should have potential applications in broadly tunable laser sources, interesting optical luminescent materials and broadband optical amplification in low-loss telecommunication windows.

(Some figures in this article are in colour only in the electronic version)

1. Introduction

Glasses and crystals doped with rare-earth (RE) metal ions are still attractive as a possible active media for solid state lasers, operating in the visible, near-infrared (NIR) and infrared (IR) spectral region. Recently, the development of Er^{3+} lasers, amplifiers and up-converters in optical fibers for telecommunications gives rise to intensive spectroscopic investigations of different Er^{3+}-doped materials [1–5]. When erbium is incorporated as an impurity into a dielectric host it usually takes the trivalent charge state. The ground state of the erbium ion with electronic configuration [Xe] $4f^{11}$ is shielded from the outer matrix by two closed 5s and 5p shells. The 4f electrons interact by spin–spin and spin–orbit interaction. As doped in a solid, the 16-fold degeneracy of the ground $^4I_{15/2}$ manifold of Er^{3+} is partially lifted by the crystal field created by the ligands (it also should be emphasized that Er^{3+} is a Kramers' ion, and split energy levels are at least twice-degenerated). As a result, rather sharp optical 4f transitions can

[5] Author to whom any correspondence should be addressed.

be achieved from erbium-doped materials. Moreover, due to its unique electronic properties, erbium is an interesting probe for a large variety of physical effects [6]. The Er^{3+} ions in glasses and crystals exhibit IR eye-safe laser emission at $\lambda = 1.5\ \mu m$ ($^4I_{13/2} \rightarrow {}^4I_{15/2}$ transition) and $\lambda = 2.9\ \mu m$ ($^4I_{11/2} \rightarrow {}^4I_{13/2}$ transition) for different technical and biomedical applications. The Er^{3+} ions also exhibit green ($\lambda_{em} = 550$ nm, $^4S_{3/2} \rightarrow {}^4I_{15/2}$ transition), red ($\lambda_{em} = 660$ nm, $^4F_{9/2} \rightarrow {}^4I_{15/2}$ transition) and NIR ($\lambda_{em} = 850$ nm, $^4S_{3/2} \rightarrow {}^4I_{13/2}$ transition and $\lambda_{em} = 1.2\ \mu m$, $^4S_{3/2} \rightarrow {}^4I_{11/2}$ transition) Stokes emissions that also can be used for laser generation [7–10]. Furthermore, within the Er^{3+} energy level scheme, several upconversion processes can take place resulting in visible anti-Stokes emission. Particularly, the glasses and disordered crystals, activated with Er^{3+} ions are prospective materials for active elements for up-converted green lasers with LED pumping in the 800–970 nm spectral range. For these reasons, the optical properties of Er^{3+}-doped crystals and glasses have been extensively investigated during recent years. Since the shape of the photoluminescence emission spectrum from Er^{3+} ions is directly related to the surrounding environment of the ions, this aspect can be tuned by varying the glass composition [11]. That is one reason, amongst others, why multi-component glasses are very interesting as hosts for RE ions in telecommunication technology. The host material for Er^{3+} ions plays an important role in obtaining a high-efficient upconversion signal, since a glass host with low phonon energy can reduce the multiphonon relaxation (MPR) and thus achieve strong upconversion luminescence. The sensitization of Er^{3+}-doped materials with Yb^{3+} ions is a well-known method for increasing the optical pumping efficiency because of the efficient energy transfer from Yb^{3+} to Er^{3+} ions, but in Er^{3+}/Yb^{3+}-codoped glass, there exists an optimal Yb^{3+} doping content [12]. Pulsed and continuous wave laser action has been demonstrated in Er^{3+}/Yb^{3+}-codoped glass lasers [13–15]. One of the interesting RE ions is Nd^{3+}, whose lasing and light amplification in the glass host has been known and exploited for years [16, 17]. Neodymium-glass lasers are employed to produce ignition in nuclear fusion research; high-power lasers have found numerous applications in materials processing, and femtosecond mode-locked lasers have recently become commercially available. All these types of Nd-glass lasers use fluorophosphate glass and can operate at 1050–1070 nm. Due to the commercial and technological importance of Nd-glass lasers, a large number of Nd-doped glasses have been investigated over the years. A new insight into the behavior of the Nd^{3+} ion in a glass host has the potential to advance the science and technology of Nd-doped glass lasers. The energy diagram of the Nd^{3+} ion is very 'dense' in terms of the number of possible states, so that various types of transitions between them, including upconversion, take place. Although a large number of emission lines have been observed to date, only the 1.06 μm band has found widespread commercial applications. Among RE ions, Pr^{3+} is an attractive optical activator, which offers the possibility of simultaneous blue, green and red emission for laser action as well as IR emission for optical amplification [18]. 1.3 μm Pr^{3+}: ZBLAN optical fiber amplification has been demonstrated [19]. 491, 520 and 635 nm upconversion lasers have been realized in Pr^{3+}: ZBLAN under a infrared laser pump [20] indicates that it is an attractive upconversion laser media. Energy transfer and yellow-to-blue frequency upconversion have been studied in Pr^{3+}-doped with other materials, including fluorophosphates [21], aluminum fluoride glasses [22] and KPb_2Cl_5 crystal [23]. These studies are important in realizing upconversion laser emission and in optimizing laser efficiency. The trivalent holmium (Ho^{3+}) is a promising ion for upconversion applications because of its energy level arrangements that allow a potential amount of an upconversion process especially in optical materials with low energy phonons. A variety of energy levels are not that significantly influenced by multiphonon decay and, therefore, that could act as initial level for the upconversion and excited state absorption (ESA) transitions, which populate higher energy levels. Ho^{3+}-doped optical materials are expected to demonstrate prominent fluorescence or lasing action at 2.08 μm, which is an eye-safe wavelength region finding applications in biomedical and sensing fields. Spectral properties of Ho^{3+} in other different inorganic glasses have been reported in literature [24–26]. In recent years, a great deal of research work has been carried out to identify new optical glasses, having potential applications in photonics. These materials are very attractive since they could be prepared in different shapes and sizes and can accept rare-earth (RE) ions without inducing any crystallization. It was found that germanate glasses have smaller maximum vibrational frequencies than those shown by silicate, phosphate and borate glasses [27–30]. The reduced phonon energy increases the quantum efficiency of luminescence from excited states of RE ions in these matrices and provides the possibility to develop a more efficient medium for optical lasers and fiber optical amplifiers [31, 32]. In this paper, we report the detailed spectral properties of Er^{3+}, Nd^{3+}, Pr^{3+} and Ho^{3+}-doped alkali fluoride zinc boro germanate glasses.

2. Experimental studies

2.1. Glass preparation

Following are the Er^{3+}, Er^{3+}/Yb^{3+}, $Nd^{3+}Pr^{3+}$ and Ho^{3+}-ions-doped alkali fluoride zinc boro germanate glasses that are developed for the present work, along with a reference glass.

$$50GeO_2–20B_2O_3–10ZnO–20LiF(\text{host glass})$$

$$50GeO_2–20B_2O_3–10ZnO–20LiF–1.0Er_2O_3$$

$$50GeO_2–20B_2O_3–10ZnO–20LiF–1.0Er_2O_3–2.0Yb_2O_3$$

$$50GeO_2–20B_2O_3–10ZnO–20LiF–1.0Nd_2O_3$$

$$50GeO_2–20B_2O_3–10ZnO–20LiF–1.0Pr_6O_{11}$$

$$50GeO_2–20B_2O_3–10ZnO–20LiF–1.0Ho_2O_3.$$

The starting materials used in the present work were reagent grade GeO_2, H_3BO_3, ZnO, LiF, Er_2O_3, Yb_2O_3, Nd_2O_3, Pr_6O_{11}

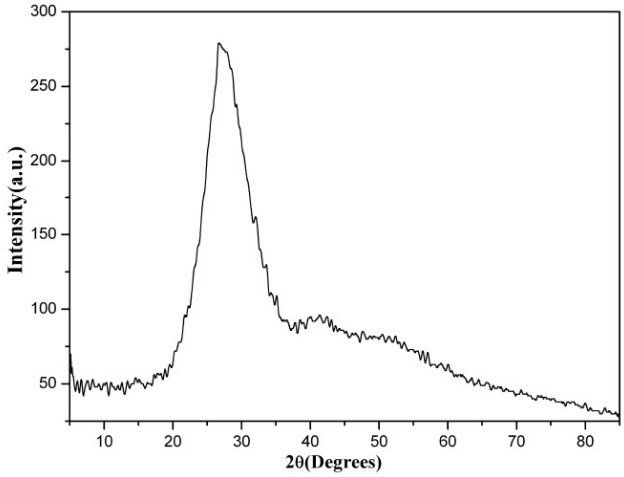

Figure 1. XRD spectrum of the $50GeO_2$–$20B_2O_3$–10ZnO–20LiF glass.

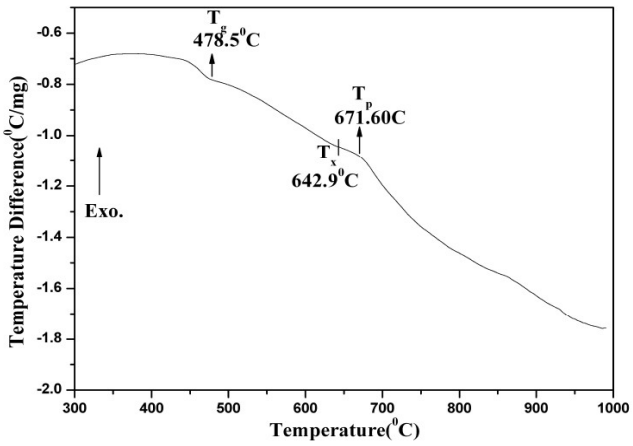

Figure 2. DTA profile of the $50GeO_2$–$20B_2O_3$–10ZnO–20LiF glass.

and Ho_2O_3. All weighed chemicals were fine powdered and mixed thoroughly before each batch (20 g) was melted at 1150 °C for 30 min in a covered corundum crucible, in air. These melts were poured onto a cold brass plate and then pressed by another plate. The obtained glasses were in the form of circular disks having 2–3 cm diameter with a thickness of about 0.3 cm and with a good transparency. All the glasses were annealed at 300 °C for 2 h to remove thermal strains.

2.2. Measurements

Glass densities were measured with toluene as the immersion liquid using Archimedes's principle. An Abbe refractometer was used to measure the refractive indices at the Na (589.3 nm) lamp wavelength. The powder x-ray diffraction (XRD) spectrum was obtained on a Rigaku D/MAX-RA diffractometer with a Ni-filter and Cu Kα (=1.542 Å) radiation with an applied voltage of 340 kV and 20 mA anode current, calibrated with Si at a rate of 2 °C min^{-1}. Differential thermal analysis (DTA) measurement was carried out on a SDT Q600 in the temperature range 30–1000 °C, at a rate of 10 °C min^{-1}, under a N_2-gas atmosphere. The UV–vis/NIR absorption spectra were measured by a Hitachi F-4100 double beam spectrophotometer. The photoluminescence spectra were measured by a Hitachi F-4500 fluorescence spectrophotometer with a 450 W xenon lamp as the excitation source. The NIR fluorescence spectrum for Nd^{3+}-ions-doped glass was obtained with a TRIAX spectrofluorimeter upon excitation with an 800 nm LD. The NIR fluorescence spectra for Er^{3+} and Er^{3+}/Yb^{3+}-ions-doped glasses were measured with a TRIAX spectrofluorimeter upon excitation with a 980 nm laser diode. The visible and NIR luminescence decay curves were recorded by using a FLS920 fluorescence spectrophotometer. The temporal decay curves of the fluorescence signals were stored by using the attached storage digital oscilloscope. The relative error in the measurement of fluorescence lifetime is estimated to be ±2%. For data fitting processes also, the error is ±2%. In, addition systematic errors have been removed through the standard instrument corrections All the measurements were carried out at room temperature.

3. Results and discussion

Figure 1 presents the XRD pattern of the $50GeO_2$–$20B_2O_3$–10ZnO–20LiF glass, which confirms its amorphous nature. Figure 2 presents the DTA thermogram of the host glass. A powder with average particle size of 200 μm from the annealed clear glass was measured by means of differential thermal analysis (DTA) measurement. From this the glass transition temperature (T_g = 478.5 °C, i.e., as determined by the inflection point at a temperature difference step change), the onset crystallization temperature (T_x = 642.9 °C), the glass thermal stability ($\Delta T = T_x$–T_g = 164.4 °C) and the exothermal peak temperature (T_p = 671.6 °C) were obtained. The thermal stability of the glasses is an important property both fundamentally and technologically. It is a measure of the degree of disorder of the glassy state. During the fiber fabrication process the preform is subjected to various heating cycles above T_g. If the glass has a poor thermal stability, then crystallization occurs in the glasses during the heating cycles. The crystals thus formed scatter the input signals and contribute to attenuation rather than amplification. Thus, evaluation of the thermal stability of the glass is important to examine its suitability to be used as an optical fiber. The thermal stability of glasses against crystallization could be evaluated from the characteristic temperatures, T_g and T_c determined from the DTA curves. The larger differences between crystallization and glass transition temperatures, and the smaller differences between crystallization and melting temperatures slow down the crystallization process and facilitate glass formation. The obtained glass stability factor reveals that these glasses are more stable. Therefore the studied glasses can be easily drawn into fibers.

3.1. Er^{3+}

Figure 3 shows the absorption spectra of Er^{3+} and Er^{3+}/Yb^{3+}-doped glasses. From these spectra, absorption bands at 407 nm,

Table 1. Measured and calculated oscillator strengths ($f \times 10^{-6}$) and JO intensity parameters of 1.0 mol% Er^{3+}-doped glass.

Upper level for the transitions from $^4I_{15/2}$	Energy (cm^{-1})	f_{exp} (10^{-6})	f_{cal} (10^{-6})	f_{cal} (10^{-6})
$^4F_{5/2}$	22 148	1.869	2.334	1.027
$^4F_{7/2}$	20 450	1.807	7.063	4.616
$^2H_{11/2}$	19 231	6.121	6.113	6.157
$^4S_{3/2}$	18 382	16.009	1.906	Excluded
$^4F_{9/2}$	15 326	7.955	6.481	7.374
$^4I_{9/2}$	12 555	1.922	0.544	1.007
$^4I_{11/2}$	10 272	1.395	1.9921	0.870
$^4I_{13/2}$	6549	5.170	4.707	2.453
			$\Omega_2 = 2.066 \times 10^{-20}$ cm^2, $\Omega_4 = 3.538 \times 10^{-20}$ cm^2, $\Omega_6 = 4.758 \times 10^{-20}$ cm^2	$\Omega_2 = 6.454 \times 10^{-20}$ cm^2, $\Omega_4 = 6.630 \times 10^{-20}$ cm^2, $\Omega_6 = 2.093 \times 10^{-20}$ cm^2

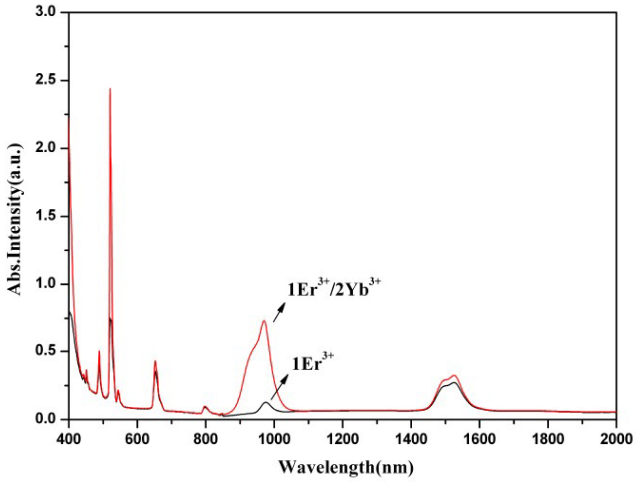

Figure 3. Absorption spectra of $1Er^{3+}$, $1Er^{3+}/2Yb^{3+}$ (mol%)-doped glasses.

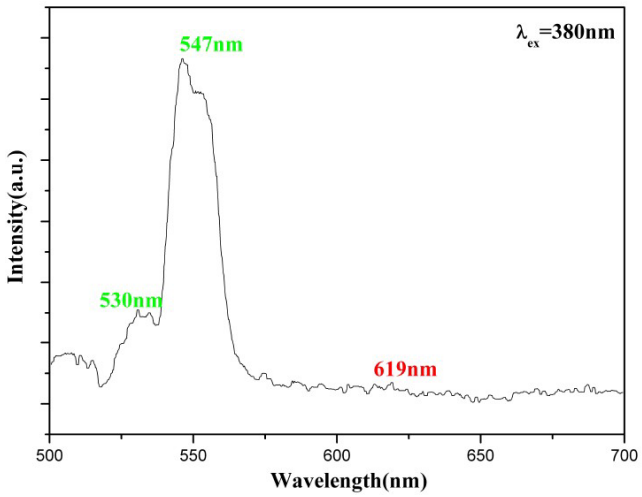

Figure 5. Emission spectrum of 1 mol% Er^{3+}-doped glass with 380 nm excitation.

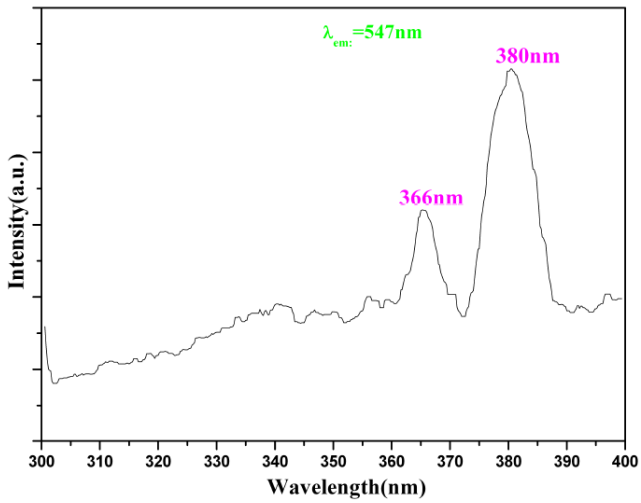

Figure 4. Excitation spectrum of 1 mol% Er^{3+}-doped glass.

443 nm, 451 nm, 487 nm, 521 nm, 543 nm, 652 nm, 796 nm, 973 nm and 1525 nm which could be assigned to $^2H_{9/2}$, $^4F_{3/2}$, $^4F_{5/2}$, $^4F_{7/2}$, $^2H_{11/2}$, $^4S_{3/2}$, $^4F_{9/2}$, $^4I_{9/2}$, $^4I_{11/2}$ and $^4I_{13/2}$ from ground state $^4I_{15/2}$, respectively, are well resolved. We have applied a least square fitting procedure to determine the JO intensity parameters Ω_2, Ω_4 and Ω_6 [33, 34] by using the experimentally measured oscillator strengths and the values obtained are presented in table 1. The intensity parameters determined in the present investigation are found to be in the order $\Omega_2 < \Omega_4 < \Omega_6$ as shown in table 1. Generally, the Ω_2 parameter is sensitive to the symmetry of the rare-earth site and strongly affected by covalency between rare-earth ions and ligand anions, where as Ω_4 and Ω_6 are related to the rigidity of the host medium in which the ions are situated. Figure 4 presents the excitation spectrum of the Er^{3+}-doped glass, monitoring emission at 547 nm. Two excitation bands at 366 nm ($^4I_{13/2} \rightarrow {}^4G_{9/2}$) and 380 nm ($^4I_{13/2} \rightarrow {}^4G_{11/2}$) are observed from this spectrum. Figure 5 shows the emission spectrum of Er^{3+}-doped glass with an excitation wavelength 380 nm, from which a strong emission band at 547 nm ($^4S_{3/2} \rightarrow {}^4I_{15/2}$) and two more weak emission bands at 530 nm ($^2H_{11/2} \rightarrow {}^4I_{15/2}$) and 619 nm ($^4F_{5/2} \rightarrow {}^4I_{13/2}$), respectively are observed. Figure 6 presents the decay curve of the emission band $^4S_{3/2} \rightarrow {}^4I_{15/2}$ of Er^{3+} with an excitation at 380 nm with a lifetime $\tau = 135$ μs. The near-infrared fluorescence

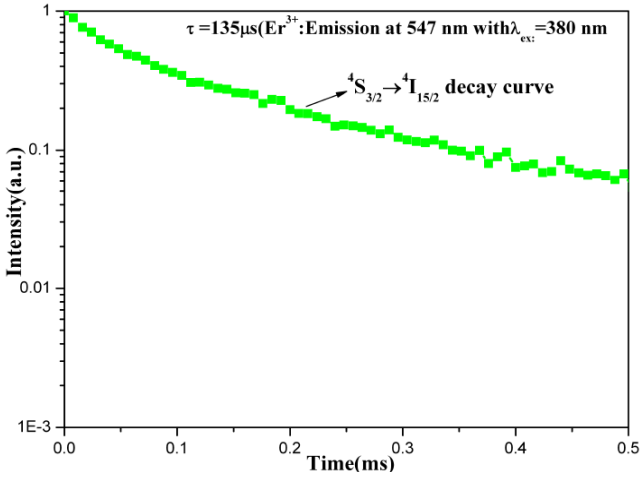

Figure 6. Decay curve of the 547 nm emission transition of Er^{3+}-doped glass. (*Y* axis on semilog scale.)

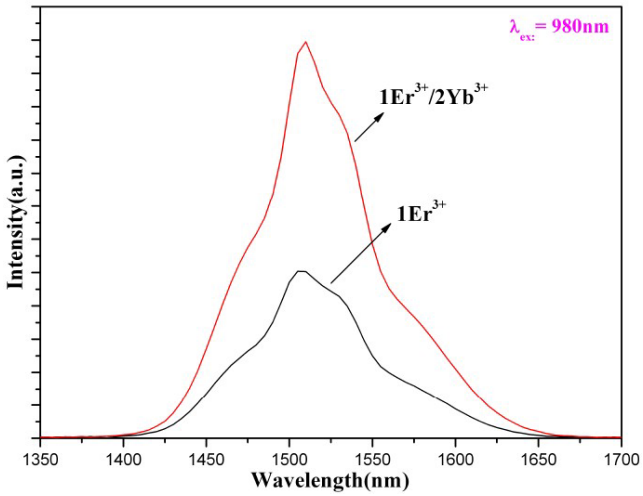

Figure 7. Near-infrared emission spectra of $1Er^{3+}$, $1Er^{3+}/2Yb^{3+}$ (mol%)-doped glasses with 980 nm LD excitation.

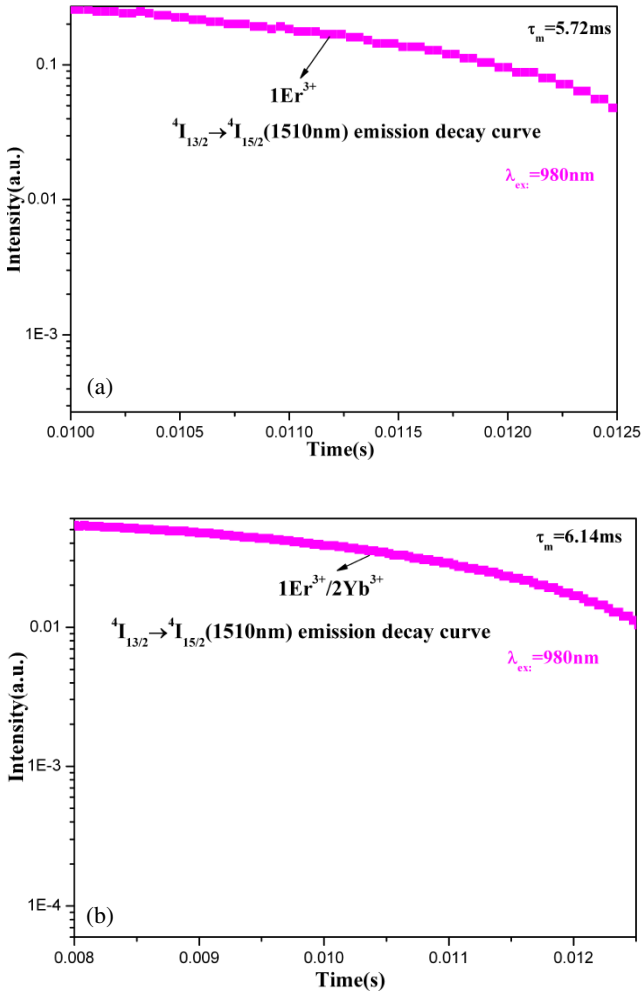

Figure 8. Decay profiles of $^4I_{13/2}$ state of Er^{3+} in (a) Er^{3+} and (b) $Er^{3+}/2Yb^{3+}$ (mol%)-doped glasses with 980 nm LD excitation. (*Y* axis on semilog scale.)

spectra of Er^{3+} and Er^{3+}/Yb^{3+}-doped glasses measured at 1.5 μm corresponding the $^4I_{13/2} \rightarrow {}^4I_{15/2}$ transition upon 980 nm laser excitation are shown in figure 7. The 980 nm laser excitation wavelength corresponds to the $^4I_{11/2} \rightarrow {}^4I_{15/2}$ state, which in turn nonradiatively relaxes to $^4I_{13/2}$. From this state, only the radiative emission to the $^4I_{15/2}$ ground state is possible, since the energy gap is nearly $\sim$6500 cm^{-1}. From these spectra, a broad near-infrared emission centered at 1510 nm ($^4I_{13/2} \rightarrow {}^4I_{15/2}$) with full width at half maximum 85 nm for Er^{3+} and 95 nm for Er^{3+}/Yb^{3+}-codoped glasses has been obtained. The 1.51 μm emission of the Er^{3+} has been observed to have several bands, which corresponded to transitions from different $^4I_{13/2}$ Stark-split levels to the ground level. Similarly, the absorption spectrum corresponding to transition from the ground level to different $^4I_{13/2}$ Stark-split levels also consisted of several bands. In a different local environment, such sub-emission (or absorption) bands might present different relative intensities. Because of the differences of the emission spectra of the different glass hosts, FWHM is often used as a semi-quantitative indication of the bandwidth. The width of the emission band $\Delta\lambda_{eff}$ for Er^{3+} ions at 1.5 μm is an important parameter for the erbium-doped fiber amplifier (EDFA) used in the wavelength-division-multiplexing (WDM) network system of optical communication. In order to satisfy the need for increased information capacity and to improve the performance of the WDM network, a medium with a wide and flat gain at 1.5 μm, which is related to the width of the emission band, is required for the EDFA [35]. It has been reported so far that the values of FWHM of 1.5 μm are 44 nm, 65 nm, 79 nm, 53 nm, 37 nm, 85 nm, 40 nm and 82 nm for Al/P silica [36], fluorozirconate [37, 38], bismuth borate glass [39], germanate glass [40], phosphate glass [41], tellurite glass [42], silica glass [43] and ZBLAN glass [44] respectively. Currently, the silica-based and ZBLAN glasses are widely used as the media of the EDFA. As already mentioned, the $\Delta\lambda_{eff}$ value of the silica-based and ZBLAN glasses are about 40 and 82 nm, respectively. The results of the spectral experiments show that the Er^{3+} and Er^{3+}/Yb^{3+}-doped alkali fluoride zinc boro germanate glasses prepared by us have an emission bands wider than that of the silica and ZBLAN glasses at 1.5 μm. Figures 8(a) and (b) shows the luminescence decay

Table 2. Spectroscopic parameters of the 1.5 μm emission for Er^{3+} in the investigated Er^{3+} and Er^{3+}/Yb^{3+} glasses, fluorosilicate and ZBLAN hosts.

Hosts	$\sigma \times 10^{21}$ (cm^{-1})	τ (ms)	$\Delta\lambda_p$ (nm)	$\sigma\tau \times (10^{24})$ (cm^2 s)	$\sigma\Delta\lambda \times$ (10^{28}) (cm^2)
Er^{3+}glass[a]	5.447	5.72	85	31.16	463
Er^{3+}/Yb^{3+}glass[a]	4.540	6.14	95	27.87	431.3
Fluorosilicate[b]	7.5	11.0	53	82.5	398
ZBLAN[b]	5.1	9.5	65	49	331

[a] In the present work.
[b] See [47].

curves of the $^4I_{13/2}$ state of Er^{3+} in Er^{3+} and Er^{3+}/Yb^{3+}-codoped glasses by monitoring the $^4I_{13/2} \rightarrow {}^4I_{15/2}$ emission of Er^{3+}. In low Er^{3+} ions content glasses, there is a lower probability of nonradiative relaxation by ion–ion interaction. The fluorescence decay time of the $^4I_{13/2} \rightarrow {}^4I_{15/2}$ transition increases from 5.72 to 6.14 ms with the addition of 2 mol% Yb^{3+} ions. The increment in the fluorescence lifetime of the $^4I_{13/2}$ level is the result of the concentration optimization of the acceptor. The concentration effect is explained by differential site occupancy and by the presence of the radiation trapping effect. In this phenomenon, photons spontaneously relaxing from the $^4I_{13/2}$ level are re-absorbed by the neighboring ions in the ground state ($^4I_{15/2}$). This process of re-absorption and re-emission is repeated and the overall result is an increase in the lifetime in comparison with a single isolated ion. The emission cross-section is an important parameter and its value signifies the rate of energy extraction from the optical material. From the emission bands the stimulated emission cross-section σ_p^E could be estimated by

$$\sigma_p^E = \frac{\lambda_p^4}{8\pi c n_d^2 \Delta\lambda_p \tau_m} \quad (1)$$

where c is the light velocity, n_d is the refractive index, λ_p is the emission peak wavelength, $\Delta\lambda_p$ is the width of the emission band, which could be calculated by integrating the intensity of the luminescence line shape and dividing it by the intensity at the peak wavelength, and τ_m is the measured lifetime [45]. The features of the Er^{3+} infrared emission are strongly dependent on the glassy-host structure. In particular the broadband emission profile, the decay time and the quantum efficiency are crucial properties for applications as optical amplifiers. For an amplifier device, the figure-of-merit is defined as the product of lifetime and emission cross-section, $\sigma\tau$. The gain bandwidth of an amplifier is determined largely by the width of the emission bandwidth and the value of the emission cross-section, $\sigma\Delta\lambda_p$ [46]. The corresponding spectroscopic parameters of the 1.5 μm emission for Er^{3+} in the investigated samples and other optical hosts are listed in table 2. It reveals that the studied Er^{3+} and Er^{3+}/Yb^{3+} glasses have superior near-infrared emission gain bandwidths compared to fluorosilicate and typical ZBLAN glasses [47]. The 1.51 μm luminescence quantum efficiency of Er^{3+} could be calculated from the following expression: $\eta = \tau A$, where τ is the measured lifetime and A is the spontaneous radiative probability, which could be calculated from the absorption

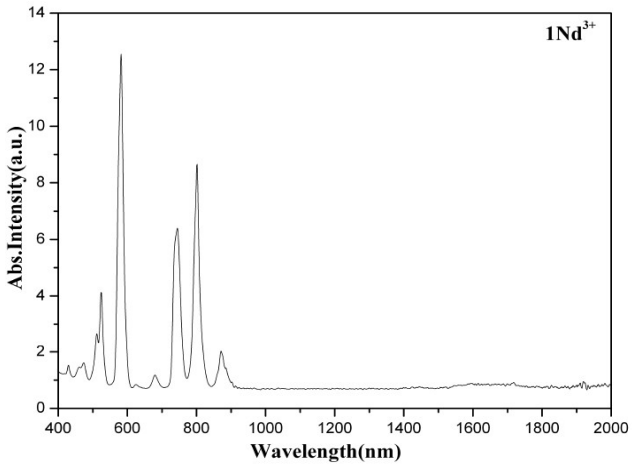

Figure 9. Absorption spectrum of 1 mol% Nd^{3+}-doped glass.

spectra of the $^4I_{15/2} \rightarrow {}^4I_{13/2}$ transition. The calculated 1.51 μm luminescence quantum efficiencies of Er^{3+} and Er^{3+}/Yb^{3+}-codoped glasses are 79% and 91%, respectively. These results clearly showed that Yb^{3+} codoping in the glass host led to longer $^4I_{13/2}$ lifetimes and higher luminescence efficiency.

3.2. Nd^{3+}

Figure 9 shows the absorption spectrum of Nd^{3+}-ion-doped glass. From this spectrum, absorption bands at 430 nm, 461 nm, 474 nm, 512 nm, 524 nm, 582 nm, 625 nm, 680 nm, 745 nm, 802 nm, 871 nm and 1607 nm, which could be ascribed to the following Nd^{3+} transitions: $^4I_{9/2} \rightarrow {}^2P_{1/2}$, $^4I_{9/2} \rightarrow {}^2K_{15/2} + {}^4G_{11/2}$, $^4I_{9/2} \rightarrow {}^2D_{3/2} + {}^2G_{9/2}$, $^4I_{9/2} \rightarrow {}^4G_{9/2} + {}^2K_{13/2}$, $^4I_{9/2} \rightarrow {}^4G_{7/2}$, $^4I_{9/2} \rightarrow {}^4G_{5/2} + {}^2G_{7/2}$, $^4I_{9/2} \rightarrow {}^2H_{11/2}$, $^4I_{9/2} \rightarrow {}^4F_{9/2}$, $^4I_{9/2} \rightarrow {}^4F_{7/2} + {}^4S_{3/2}$, $^4I_{9/2} \rightarrow {}^4F_{5/2} + {}^2H_{9/2}$, $^4I_{9/2} \rightarrow {}^4F_{3/2}$ and $^4I_{9/2} \rightarrow {}^4I_{15/2}$, respectively, are observed. Owing to the absence of long-range order in glasses, the micro symmetry around the Nd^{3+} ions differs slightly from site to site and, therefore, the transitions are inhomogeneously broadened with typical halfwidths of about 200 cm^{-1} for isolated bands. From these transitions the calculated Judd–Ofelt parameters are listed in table 3. As usual the intensity parameters are treated as phenomenological parameters and their values were obtained by a least-squares computer program between the measured and calculated oscillator strengths. When a rare-earth ion is embedded in a glassy matrix (oxide or fluoride) a strong covalent bond will exist between the rare-earth ion and the surrounding oxygen or fluorine. The amount of covalency between these bonds can be inferred from the intensity and nature of hypersensitive transitions. It has been shown that the amount of covalency between the rare-earth ion and the surrounding ligand environment in a glass increases with the intensity of the hypersensitive transition. Since the intensity of the $^4I_{9/2} \rightarrow {}^4G_{5/2}$ hypersensitive transition of Nd^{3+} is the main determining factor for the value of the Judd–Ofelt parameter Ω_2, this parameter may also be used to monitor the covalency changes in glasses. The JO parameters in the

Table 3. Measured and calculated oscillator strengths ($f \times 10^{-6}$) and JO intensity parameters of 1.0 mol% Nd^{3+}-doped glass.

Upper level for the transitions from $^4I_{9/2}$	Energy (cm^{-1})	f_{exp} (10^{-6})	f_{cal} (10^{-6})
$^2P_{1/2}$	23 364	10.337	5.909
$^2K_{15/2} + {}^2G_{9/2} + {}^4G_{11/2} + {}^2D_{3/2}$	21 142	24.630	20.496
$^2K_{13/2} + {}^4G_{7/2} + {}^4G_{9/2}$	19 084	76.571	63.418
$^4G_{5/2} + {}^2G_{7/2}$	17182	216.94	219.974
$^2H_{11/2}$	15 974	3.129	1.715
$^4F_{9/2}$	14 706	9.321	11.622
$^4F_{7/2} + {}^4S_{3/2}$	13 423	87.062	105.415
$^4F_{5/2} + {}^2H_{9/2}$	12 469	89.876	63.321
			$\Omega_2 = 55.5 \times 10^{-20}$ cm^2, $\Omega_4 = 40.12 \times 10^{-20}$ cm^2, $\Omega_6 = 56.78 \times 10^{-20}$ cm^2

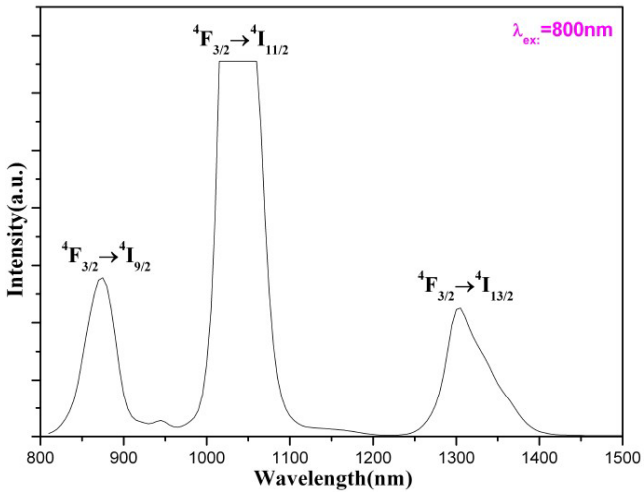

Figure 10. Near-infrared emission spectrum of 1 mol% Nd^{3+}-doped glass with 800 nm LD excitation.

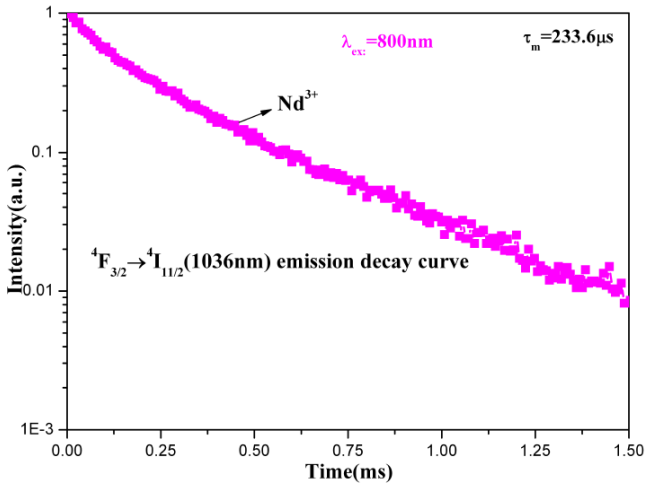

Figure 11. Decay curve of 1036 nm emission of Nd^{3+}-doped glass with 800 nm LD excitation. (Y axis on semilog scale.)

present investigation follow the trend: $\Omega_6 > \Omega_2 > \Omega_4$ in the studied glass. According to Jacobs and Weber [48], the emission intensity of the $^4F_{3/2} \rightarrow {}^4I_{11/2}$ (1.06 μm) laser transition is mainly dependent on the Ω_4 and Ω_6 parameters. For a large emission cross-section (Σ), the values of Ω_4 and Ω_6 are required to be as large as possible. Since $\|U^2\|$ values are zero because of the triangle rule $|J^1 - J\| \leqslant \lambda \leqslant |J^1 + J|$ [49], Ω_2 does not enter the branching ratio calculations of the $^4F_{3/2} \rightarrow {}^4I_J^1$ levels. Hence branching ratios can only be expressed in terms of the Ω_4/Ω_6 ratio. To obtain the maximum fluorescence intensity to the $^4F_{3/2} \rightarrow {}^4I_{11/2}$ transition it is required that $\Omega_4 \ll \Omega_6$. Following the formulae reported earlier [50] for Nd^{3+} ion, the calculated luminescent branching ratios are 0.399, 0.478, 0.119 and 0.003 for 0.9 μm, 1.06 μm, 1.35 μm and 1.9 μm near-infrared emissions, respectively. From the above calculations, as a first step one can select a material with a low 'X' (=spectroscopic quality factor, Ω_4/Ω_6) parameter value for laser action at the important 1.3 μm in the near-infrared region. Figure 10 shows the near-infrared emission spectrum of Nd^{3+}-doped glass with 800 nm LD excitation. From this spectrum a strong emission band centered at 1036 nm ($^4F_{3/2} \rightarrow {}^4I_{11/2}$) with full width at half maximum (FWHM) around 63 nm and two more emission bands centered at 876 nm ($^4F_{3/2} \rightarrow {}^4I_{9/2}$) and 1304 nm ($^4F_{3/2} \rightarrow {}^4I_{13/2}$) with FWHM around 42 nm and 65 nm respectively have also been observed and Nd^{3+}-doped materials have proven to be one of the most efficient candidates for photonic devices such as, for example, fiber lasers, micro chip lasers and planar waveguides [51–53]. Most recent research has been focused in the near-infrared spectral range, from 1000 to 1400 nm, where Nd^{3+} ions present radiative emission at 1060 and 1350 nm originating from the electronic transitions between the $4f^n$ levels, $^4F_{3/2} \rightarrow {}^4I_{11/2}$ and $^4F_{3/2} \rightarrow {}^4I_{13/2}$. In our studied Nd^{3+} glass, larger FWHM values (63 and 65 nm) are achieved at these wavelengths for the above processes. Figure 11 shows the decay curve of the 1036 nm emission band of Nd^{3+}-doped glass under 800 nm LD excitation. The measured lifetime of the 1036 nm emission band is 233.6 μs. Following the formula (1) given above we have calculated the stimulated emission cross-section of this interesting laser emission at 1036 nm for the Nd^{3+} ion and its obtained value is 3.987×10^{-20} cm^2. The calculated luminescence quantum efficiency of the $^4F_{3/2} \rightarrow {}^4I_{11/2}$ emission band at 1036 nm is 67%.

Table 4. Measured and calculated oscillator strengths ($f \times 10^{-6}$) and JO intensity parameters of 1.0 mol% Pr^{3+}-doped glass.

Upper level for the transitions from $^3H_4$	Energy (cm^{-1})	f_{exp} (10^{-6})	Modified JO theory: f_{cal} (10^{-6}), with $^3P_2$ state	Modified JO theory: f_{cal} (10^{-6}) without $^3P_2$
$^3P_2$	22 573	122.503	136.117	Excluded
$^3P_1$	21 322	61.610 4	71.147	71.563
$^3P_0$	20 704	39.527	27.485	26.629
$^1D_2$	17 007	27.289 8	32.182	44.025
$^1G_4$	9 950	4.868 08	4.456	6.078
$^3F_3 + {}^3F_4$	6 596	108.045	73.536	97.546
$^3F_2 + {}^3H_6$	5 206	26.773	32.375	22.897
			$\Omega_2 = 483.4 \times 10^{-20}$ cm^2, $\Omega_4 = 52.016 \times 10^{-20}$ cm^2, $\Omega_6 = 261.200 \times 10^{-20}$ cm^2	$\Omega_2 = 230.192 \times 10^{-20}$ cm^2, $\Omega_4 = 50.396 \times 10^{-20}$ cm^2, $\Omega_6 = 381.842 \times 10^{-20}$ cm^2

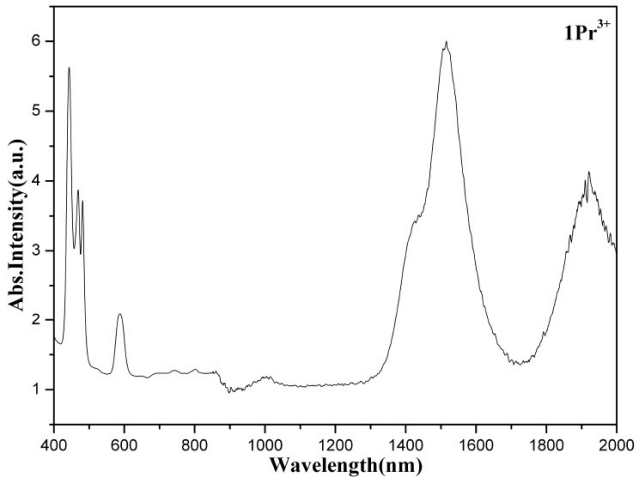

Figure 12. Absorption spectrum of 1 mol% Pr^{3+}-doped glass.

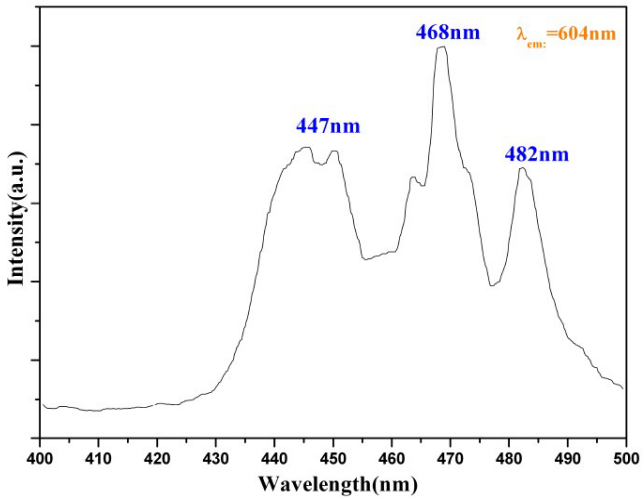

Figure 13. Excitation spectrum of 1 mol% Pr^{3+}-doped glass.

3.3. Pr^{3+}

Figure 12 presents the absorption spectrum of Pr^{3+}-doped glass. From this spectrum, absorption bands at 443 nm, 469 nm, 481 nm, 588 nm, 1516 nm and 1921 nm are observed, which could be ascribed to Pr^{3+} transitions: $^3H_4 \rightarrow {}^3P_2$, $^3H_4 \rightarrow {}^3P_1$, $^3H_4 \rightarrow {}^3P_0$, $^3H_4 \rightarrow {}^1D_2$, $^3H_4 \rightarrow {}^3F_4{}^3F_3$ and $^3H_4 \rightarrow {}^3F_2 + {}^3H_6$ respectively. All transitions in the absorption spectrum of Pr^{3+} start from the $^3H_4$ ground state. The observed absorption bands can be divided into three groups; transition from $^3H_4 \rightarrow {}^3F_{2,3,4}$ in the infrared, the $^3H_4 \rightarrow {}^1D_2$ transition at 588 nm and the $^3H_4 \rightarrow {}^3P_{0,1,2}$ complex group of transitions in violet-blue region. The last group is responsible for the blue color of Pr^{3+} ion. The bands correspond to the $4f^2$-intraconfigurational electric dipole transitions from the ground state $^3H_4$ to the excited-states $^3P_{J\,(J=0,1,2)}$ and $^1D_2$ and the band widths are due to the combination of inhomogeneous broadening and unresolved Stark splitting. From these absorption bands the calculated Judd–Ofelt parameters are presented in table 4. It should be mentioned that the hypersensitive transition $^3H_4 \rightarrow {}^3F_2$ has to be included in the fit for Pr^{3+} systems; otherwise a negative value for the Ω_2 parameter is found. To avoid this unphysical result, a modified JO theory [54] has been applied. It is interesting to note that the relation $\Omega_2 > \Omega_6 > \Omega_4$ with a $^3P_2$ state and $\Omega_6 > \Omega_2 > \Omega_4$ without a $^3P_2$ state among modified JO parameters has been found for the Pr^{3+}-doped glass. Figure 13 shows the excitation spectrum of the Pr^{3+}-ions-doped glass, monitoring emission at 604 nm. Three excitation bands at 447 nm ($^3H_4 \rightarrow {}^3P_2$), 468 nm ($^3H_4 \rightarrow {}^3P_1$) and 482 nm ($^3H_4 \rightarrow {}^3P_0$), respectively, are observed from this spectrum. From these excitation wavelengths, we have selected the 468 nm wavelength to measure the emission spectrum of Pr^{3+}-doped glass. Figure 14 presents the emission spectrum of Pr^{3+} ions with a 468 nm excitation wavelength. The detector response did not allow us to measure the emission spectra beyond 800 nm. A strong emission band at 604 nm ($^3P_0 \rightarrow {}^3H_6$) and two more weak emission bands at 526 nm ($^3P_1 \rightarrow {}^3H_5$) and 641 nm ($^3P_1 \rightarrow {}^3F_2$) are observed from this spectrum. Due to the large energy gap (3858.5 cm^{-1}) between $^3P_0$ and $^1D_2$ and the low phonon energy (800 cm^{-1}) [55], multiphonon nonradiative relaxation from ^3P to $^1D_2$ is very small, and hence the $^1D_2$ luminescence was not observed. However, when the $^1D_2$ state is excited at 588 nm, upconversion luminescence coming from $^3P_0$ can be obtained for the Pr^{3+} ions. Figure 15

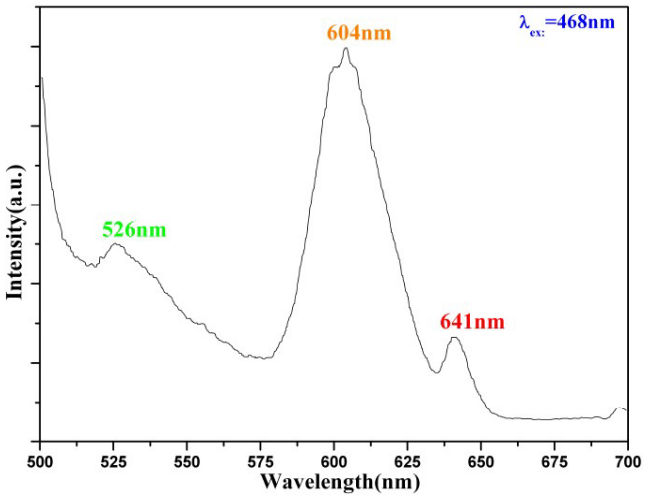

Figure 14. Emission spectrum of 1 mol% Pr^{3+}-doped glass with 468 nm excitation.

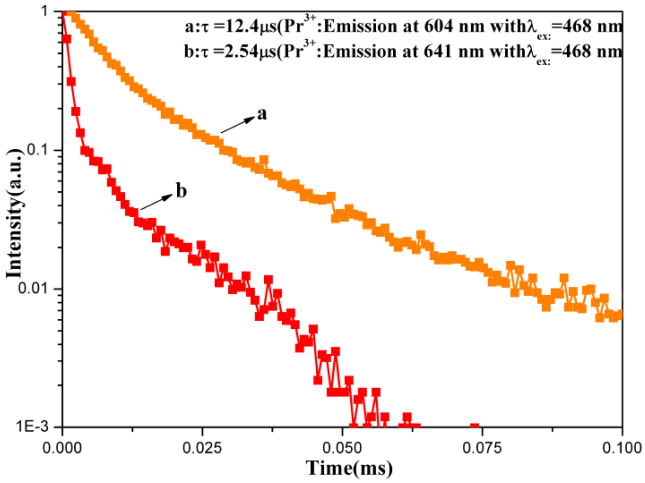

Figure 15. Decay curve of the 602 nm emission transition of Pr^{3+}-doped glass. (Y-axis on semilog scale.)

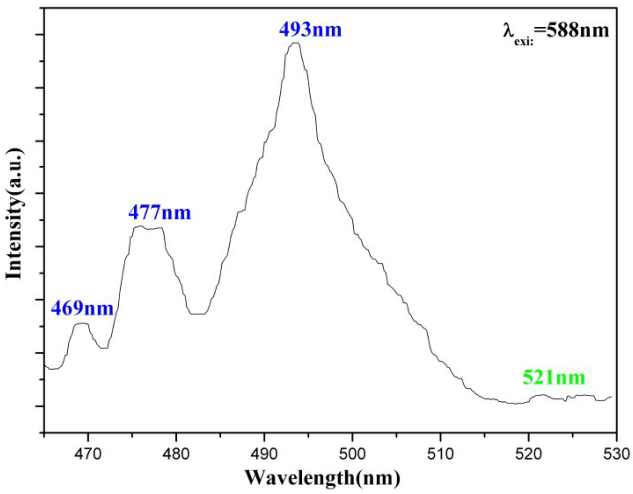

Figure 16. Upconversion emission spectrum of 1 mol% Pr^{3+}-doped glass.

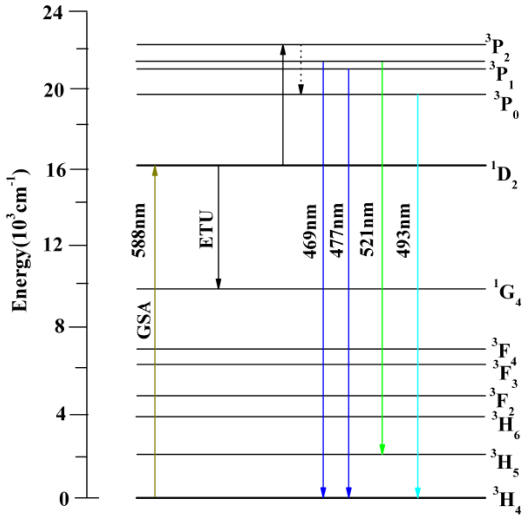

Figure 17. Energy level diagram of Pr^{3+} ions with observed upconversion emissions.

presents the decay curves of the emission bands $^3P_0 \rightarrow {}^3H_6$ (604 nm) and $^3P_1 \rightarrow {}^3F_2$ (641 nm) of Pr^{3+} with an excitation at 468 nm with lifetimes $\tau = 12.4\ \mu$s and 2.54 μs respectively. Figure 16 presents the upconversion spectrum of Pr^{3+} ions with a 588 nm excitation wavelength. Four emission bands around 469 nm, 477 nm, 493 nm and 521 nm are observed from this spectrum and could be ascribed to the $^3P_1 \rightarrow {}^3H_4$, $^3P_0 \rightarrow {}^3H_4$ and $^3P_1 \rightarrow {}^3H_5$ transitions, respectively. Based on the energy level data reported by Weber [56], the energy level diagram of Pr^{3+} ion upconversion emission transitions is presented in figure 17.

3.4. Ho^{3+}

Figure 18 presents the absorption spectrum of the 1 mol% Ho^{3+}-ions-doped glass. From this spectrum, absorption bands at 417 nm, 450 nm, 470 nm, 485 nm, 537 nm, 642 nm, 1148 nm and 1945 nm are observed and assigned to the Ho^{3+} transitions: $^5I_8 \rightarrow {}^5G_5$, $^5I_8 \rightarrow {}^5G_6$, $^5I_8 \rightarrow {}^5F_2$, $^5I_8 \rightarrow {}^5F_3$, $^5I_8 \rightarrow {}^5S_2 + {}^5F_4$, $^5I_8 \rightarrow {}^5F_5$, $^5I_8 \rightarrow {}^5I_6$ and $^5I_8 \rightarrow {}^5I_7$ respectively. From these absorption bands the calculated Judd–Ofelt parameters are listed in table 5. As Weber *et al* [57] reported, large Ω_2 values are probably caused by the relatively high covalency of the chemical bond in the glass structure. The closely spaced $^5S_2$, $^5F_4$ levels have been treated as one level for the Judd–Ofelt calculations. One of the several transitions is found to be very sensitive to the glass composition and also to the Ho^{3+} concentration. Its absorption band intensity shows a peculiar variation and is called the hypersensitive level. In our observations, one such level ($^5I_8 \rightarrow {}^5G_6$) is more intense and it obeys the selection rule ($\Delta J \leqslant 2$; $\Delta L \leqslant 2$; $\Delta S = 0$) as was described in earlier literature [58]. Figure 19 shows the excitation spectrum of Ho^{3+}-doped glass, monitoring emission at 658 nm. Three excitation bands centered at 369 nm (CT band), 401 nm ($^5I_8 \rightarrow {}^5G_4$) and 441 nm ($^5I_8 \rightarrow {}^5G_6$) are observed from this spectrum. Figure 20 presents the emission

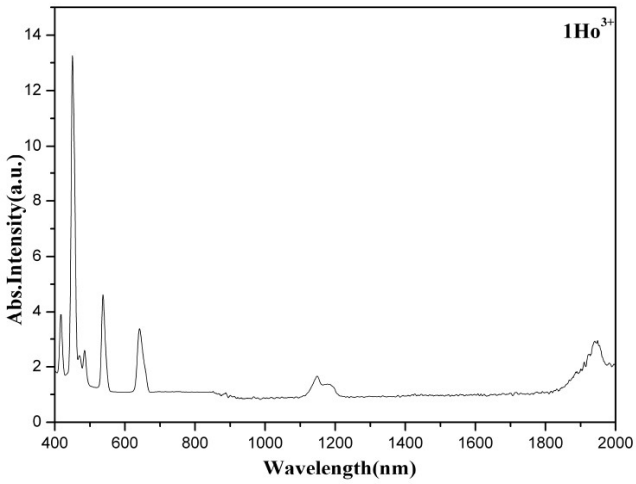

Figure 18. Absorption spectrum of 1 mol% Ho^{3+}-doped glass.

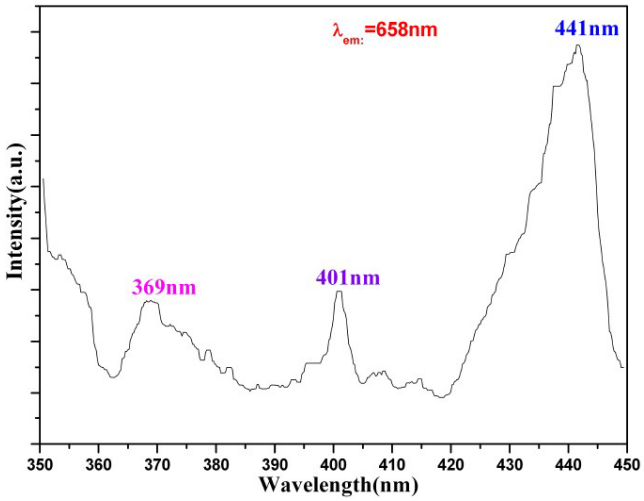

Figure 19. Excitation spectrum of 1 mol% Ho^{3+}-doped glass.

Table 5. Measured and calculated oscillator strengths ($f \times 10^{-6}$) and JO intensity parameters of 1.0 mol% Ho^{3+}-doped glass.

Upper level for the transitions from $^5I_8$	Energy (cm^{-1})	f_{exp} (10^{-6})	f_{cal} (10^{-6})
$^5G_5$	23 981	35.444	37.768
$^5G_6$	22 222	244.785	244.800
$^5F_3$	20 619	14.081	10.934
$^5S_2 + {}^5F_4$	18 622	44.536	39.152
$^5F_5$	15 576	38.337	36.566
$^5I_6$	8 711	12.066	13.217
$^5I_7$	5 155	6.664	18.145
			$\Omega_2 = 60.44 \times 10^{-20}$ cm^2, $\Omega_4 = 31.98 \times 10^{-20}$ cm^2, $\Omega_6 = 21.03 \times 10^{-20}$ cm^2

spectrum of Ho^{3+}-doped glass with a 441 nm excitation wavelength. Three emission bands at 525 nm, 555 nm and 658 nm are observed from this spectrum, which could be ascribed to the $^5F_4 \rightarrow {}^5I_8$, $^5S_2 \rightarrow {}^5I_8$ and $^5F_5 \rightarrow {}^5I_8$ transitions, respectively. Figure 21 presents the decay curve of the emission band $^5F_5 \rightarrow {}^5I_8$ of Ho^{3+} with an excitation at 441 nm with a lifetime $\tau = 90\ \mu$s. Figure 22 shows the upconversion emission spectrum of Ho^{3+}-doped glass with a 658 nm excitation wavelength. We have observed upconversion emissions at 432 nm, 468 nm, 482 nm and 505 nm from this spectrum, which could be ascribed to the $^5G_5 \rightarrow {}^5I_8$, $^5F_2 \rightarrow {}^5I_8$, $^5F_3 \rightarrow {}^5I_8$ and ($^5S_2$, $^5F_4 \rightarrow {}^5I_8$) transitions of Ho^{3+} ions, respectively. Figure 23 clearly describes the mechanism involved in the upconversion emission process upon excitation of the holmium glass with $\lambda_{ex:} = 658$ nm. The transition from the ground state $^5I_8$ to the excited level $^5F_5$ is known as ground state absorption (GSA); it then depopulates rapidly via nonradiative de-excitation down to the nearest lower metastable state $^5I_6$ level. The ions in this level further de-excite radiatively towards the $^5I_7$ and $^5I_8$ levels, or be brought by ESA (excited state absorption) to the $^5G_5$ level, from which a part of the excited ions emits towards the ground state and another part feeds into the ($^5F_4$, $^5S_2$) levels through the $^5F_3$ level via a nonradiative de-excitation. In this

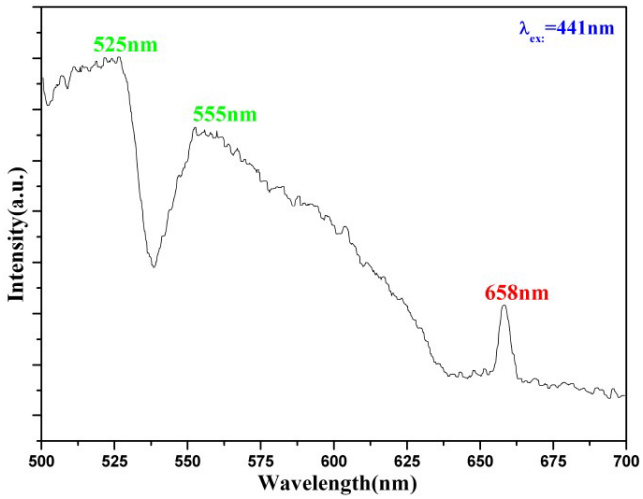

Figure 20. Emission spectrum of 1 mol% Ho^{3+}-doped glass with 441 nm excitation.

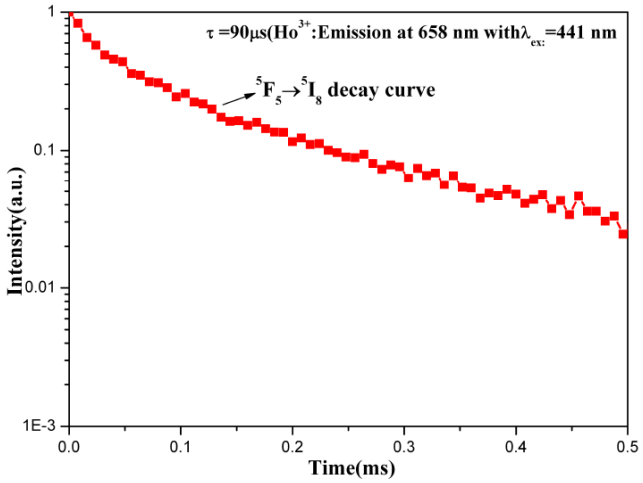

Figure 21. Decay curve of the 658 nm emission transition of Ho^{3+}-doped glass. (Y axis on semilog scale.)

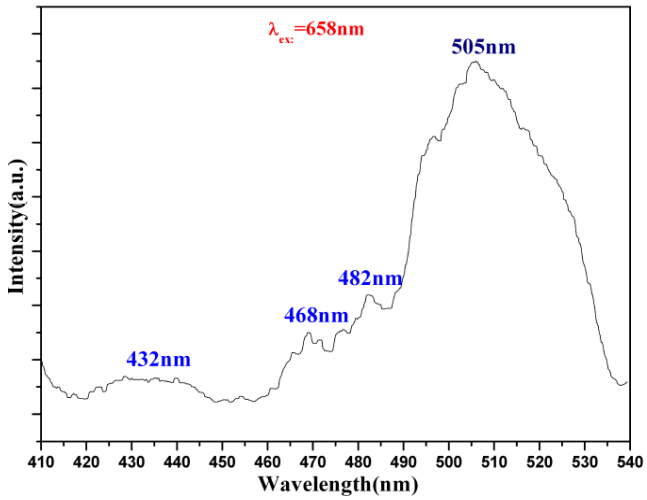

Figure 22. Upconversion emission spectrum of 1 mol% Ho^{3+}-doped glass.

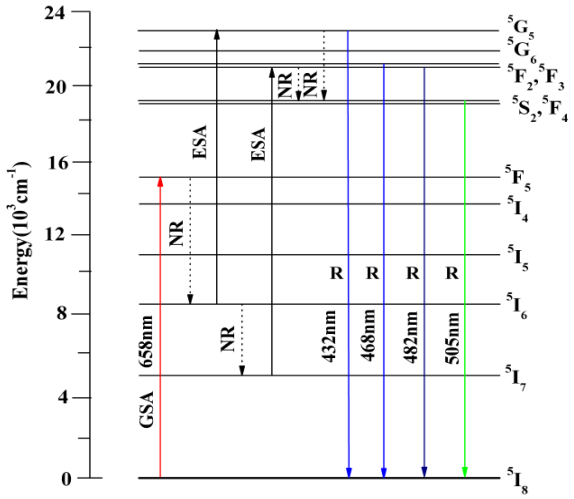

Figure 23. Energy level diagram of Ho^{3+} ions with observed upconversion emissions.

case, the $^5F_4$ and $^5S_2$ levels are thermally coupled and hence they are considered as mixed-up levels. Another similar pathway is also shown in the same figure. Starting from the $^5I_7$ level, which is mainly fed from the $^5I_6$ level, the ions in the $^5I_7$ level either de-excite radiatively towards the ground state or are re-excited to the $^5F_3$ level by ESA, from which a part of the excited ions emits and another part feeds into the $^5F_4$ upper level. Thus, upconversion emission bands measured from the Ho^{3+} glass studied here upon the excitation with $\lambda_{ex:} = 658$ nm are due to a three photon absorption process and the arrangement of energy levels of Ho^{3+} ions are indicated in figure 23. From this figure, both the radiative and nonradiative transitions are clearly marked to assist understanding.

$^5I_8 \rightarrow {}^5F_5$(GSA); $^5I_6 \rightarrow {}^5G_5$(ESA) and $^5F_3 \rightarrow {}^5I_8$(ESA)

$^5F_5 \rightarrow {}^5I_6$; $^5I_7$; $^5I_6 \rightarrow {}^5I_7$; $^5F_3 \rightarrow {}^5F_4$; $^5S_2$ and $^5G_5 \rightarrow {}^5F_4$; $^5S_2$:

4. Conclusions

In summary, alkali fluoride zinc boro germanate glasses were prepared with Er^{3+}, Nd^{3+}, Pr^{3+} and Ho^{3+} as dopant ions for characterization of their thermal and visible and near-infrared luminescence properties. For Pr^{3+} and Ho^{3+}-doped glasses, upconversion spectra are also measured with 588 and 658 nm, respectively, as excitation wavelengths, and the related mechanisms are also explained. Decay curves were measured for the visible emissions of Er^{3+}, Pr^{3+} and Ho^{3+} ions at 547 nm (Er^{3+}: green), 604 nm, 641 nm (Pr^{3+}: orange, red) and 658 nm (Ho^{3+}: red), respectively, with lifetimes 135, 12.4, 2.54 and 90 μs. The measured decay time of the $^4I_{13/2} \rightarrow {}^4I_{15/2}$ transition (at wavelength 1.510 μm) is about 5.72 ms and 6.14 ms for 1.0 Er^{3+} and 1.0 $Er^{3+}/2Yb^{3+}$ (mol%)-codoped glasses, respectively. The maximum stimulated emission cross sections for the $^4I_{13/2} \rightarrow {}^4I_{15/2}$ transition of Er^{3+} and Er^{3+}/Yb^{3+} are 5.447×10^{-21} and 4.540×10^{-21} cm^2. These glasses should have potential applications in broadly tunable laser sources, interesting optical luminescent materials and broadband optical amplification in low-loss telecommunication windows. Also, these glasses offer the advantage of high chemical stability; they can remain as long as six months in a laboratory atmosphere without visible signs of deterioration, crystallization, or hygroscopy.

Acknowledgments

This work was financially supported by the National Nature Science Foundation of China (Grant Nos 50672087 and 60778039), the National Basic Research Program of China (2006CB806007) and the National High Technology Program of China (2006AA03Z304). This work was also supported by the program for Changjiang Scholars and Innovative Research Team in University (IRT0651).

References

[1] Qiao X, Fan X P, Wang J and Wang M Q 2006 *J. Appl. Phys.* **99** 074302
[2] Shen X, Nie Q H, Xu T F and Gao Y 2005 *Spectrochim. Acta* A **61** 2827
[3] Yang Z, Xu S, Hu L and Jiang Z 2004 *J. Mater. Sci.* **39** 2223
[4] Chu S Y, Wen C H, Tyan S L, Lin Y G, Juang Y D and Wen C K 2004 *J. Appl. Phys.* **96** 2552
[5] Sun J, Zhang J, Shiluo Y, Lin J L and Song H W 2003 *J. Appl. Phys.* **94** 1325
[6] Polman A 2001 *Physica* B **300** 78
[7] Padlyak B, Vlokh O, Fabisiak F, Sagoo K and Kuklinski B 2006 *Opt. Mater.* **28** 157
[8] Szachowcz M, Taseu S, Joubert M R, Moretti R and Nim M 2006 *Opt. Mater.* **28** 162
[9] Poirier G, Jerez V A, de Araujo C B, Messaddeq Y, Ribeiro S J L and Poulain M 2003 *J. Appl. Phys.* **93** 1493
[10] Yang J H, Dai S X, Zhou Y F, Wen L, Hu L L and Jiang Z H 2003 *J. Appl. Phys.* **93** 977

[11] Enrichi F, Mattei G, Sada C, Trave E, Pacifici D, Franzo G, Priolo F, Iacona F, Falconieri M and Borsella E 2004 *J. Appl. Phys.* **96** 3925
[12] Strohhofer C and Polman A 2001 *J. Appl. Phys.* **90** 4314
[13] Laporta P, de Silvestri S, Magni V and Svelto O 1991 *Opt. Lett.* **16** 1952
[14] Hutchinson J A and Allik T H 1992 *Appl. Phys. Lett.* **60** 1424
[15] Hsu K, Miller C H, Kringlebotn J T and Payne D N 1995 *Opt. Lett.* **20** 337
[16] Weber M J 1980 *J. Non-Cryst. Solids* **42** 189
[17] Naftaly M and Jha A 2000 *J. Appl. Phys.* **87** 2098
[18] Kaminskii A A 1991 *Ann. Phys. (Paris)* **16** 639
[19] Lobbett R, Wyatt R, Eardley P, Whitley T J, Smyth P, Szebesta D, Carter S F, Davey S T, Millar C A and Brierley M C 1991 *Electron. Lett.* **27** 1472
[20] Pask H M and Hanna A C 1997 *Opt. Commun.* **134** 139
[21] Balda R, Fernández J, Adam J L, Mendioroz A and Arriandiaga M A 1999 *J. Non-Cryst. Solids* **256/257** 299
[22] Rolli R, Ronchin S, Montagna M, Moser E, Duverger C, Tikhomirov V K, Jha A and Ferrari M 2001 *J. Non-Cryst. Solids* **280** 269
[23] Balda R, Voda M, Al-Saleh M and Fernández J 2002 *J. Lumin.* **97** 190
[24] Reisfield R and Hormadaly J 1976 *J. Chem. Phys. Acta* **64** 3207
[25] Rai S B 2002 *Spectrochim. Acta* A **58** 1 559
[26] Prasad N V V, Annapurna K, Sooraj Hussain N and Buddhudu S 2003 *Mater. Lett.* **57** 2071
[27] Balda R, Fernández J, de Pablos A and Fdez-Navarro J M 1999 *J. Phys.: Condens. Matter* **11** 411
[28] Pan Z, Morgan S H, Loper A, King V, Long B H and Collins W E 1995 *J. Appl. Phys.* **77** 4688
[29] Wachtler M, Speghini A, Pigorini S, Rolli R and Bettinelli M 1997 *J. Non-Cryst. Solids* **217** 111
[30] Ribeiro S J L, Dexpert-Ghys J, Piriou B and Mastelaro V R 1993 *J. Non-Cryst. Solids* **159** 213
[31] Canale J E, Condrate R A, Nassau Sr K and Cornilsen B C 1986 *J. Can. Ceram. Soc.* **55** 50
[32] Wang J, Lincoln J R, Brocklesby W S, Deol R S, Mackechnie C J, Pearson A, Tropper A C, Hanna D C and Payne D N 1993 *J. Appl. Phys.* **73** 8066
[33] Judd B R 1962 *Phys. Rev.* **127** 750
[34] Ofelt G S 1962 *J. Chem. Phys.* **37** 511
[35] Chen Y, Huang Y, Huang M L, Chen R P and Luo Z 2004 *Opt. Mater.* **25** 271
[36] Miniscalco W J 1993 *Rare-Earth Doped Fiber Lasers and Amplifiers* ed M J F Diggonet (New York: Dekker)
[37] Miniscalco W J 1991 *J. Lightwave Technol.* **9** 234
[38] Semenkoff M, Guibert M, Ronarch D, Sorel Y and Kerdiles J F 1995 *J. Non-Cryst. Solids* **184** 240
[39] Yang J, Dai S, Zhou Y F, Wen L, Hu L L and Jiang Z 2003 *J. Appl. Phys.* **93** 977
[40] Lin H, Pun E Y B, Man S Q and Liu X R 2001 *J. Opt. Soc. Am.* B **18** 602
[41] Jiang S, Luo T, Hwang B C, Smekatala F, Seneschal K, Lucas J and Peyghambarian N 2000 *J. Non-Cryst. Solids* **263–264** 364
[42] Mori A and Ohishi Y 1998 *Optical Fiber Communication Conference (OFC)* (*OSA Technical Digest Series* vol 6) (California: Optical Society of America) Paper WA1
[43] Zou X and Izumitani T 1993 *J. Non-Cryst. Solids* **162** 68
[44] Wetenkamp L, West G F and Tobben H 1992 *J. Non-Cryst. Solids* **140** 35
[45] Karthikeyan B, Mohan S and Baesso M L 2003 *Physica* B **337** 249
[46] Shen S and Jha A 2004 *Opt. Mater.* **25** 321
[47] Jha M, Shen S and Naftaly M 2000 *Phys. Rev.* B **62** 6215
[48] Jacobs R and Weber M J 1976 *IEEE J. Quantum Electron.* **12** 102
[49] Reisberg L A and Weber M J 1975 *Relaxation Phenomena in Rare Earth Luminescence in Progress in Optics* vol XIV, ed E Wolf (Amsterdam: North-Holland)
[50] Lomheim T S and De Shazer L G 1978 *Opt. Commun.* **24** 89
[51] Lim K S, Lee C W and Kim S T 2000 *J. Lumin.* **87–89** 1008
[52] Courrol L C, Maldonado E P, Gomes L and Vieira N D 2000 *Opt. Mater.* **14** 81
[53] Serqueira E O, Dantas N O, Monte A F G and Bell M J V 2006 *J. Non-Cryst. Solids* **352** 3628
[54] Dunina E B, Kaminskii A A, Kornienko A A, Kurbanov K and Pukhov K K 1990 *Sov. Phys.—Solid State* **32** 290
[55] Chen Y and Auzel F 1995 *J. Non-Cryst. Solids* **184** 278
[56] Weber M J 1968 *J. Chem. Phys.* **48** 4774
[57] Weber M J, Ziegler D C and Angell C A 1982 *J. Appl. Phys.* **53** 4344
[58] Jorgenson C K and Judd B R 1964 *J. Mol. Phys.* **8** 281